Ground State Properties of the *A*-site Ordered Manganites, RBaMn$_2$O$_6$ (R = La, Pr and Nd)

Tomohiko Nakajima[1]*, Hiroshi Kageyama[1], Hideki Yoshizawa[2], Kenji Ohoyama[3] and Yutaka Ueda[1]

[1]*Materials Design and Characterization Laboratory, Institute for Solid State Physics, University of Tokyo,*
5-1-5 Kashiwanoha, Kashiwa, Chiba 277-8581
[2]*Neutron Science Laboratory, Institute for Solid State Physics, University of Tokyo, 106-1 Shirakata, Tokai, Ibaraki 319-1106*
[3]*Institute for Materials Research, Tohoku University, 2-1-1 Katahira, Aoba-ku, Sendai 980-8577*

The most significant structural feature of the *A*-site ordered manganese perovskites, RBaMn$_2$O$_6$, is that the MnO$_2$ square sublattice is sandwiched by two types of rock-salt layers, RO and BaO, with much different sizes and consequently the MnO$_6$ octahedron itself is distorted in a noncetrosymmetric manner. The structures and electromagnetic properties of RBaMn$_2$O$_6$ (R = La, Pr and Nd) have been investigated. They have tetragonal structures with no tilt of MnO$_6$ octahedra and show ferromagnetic metal transitions. The ground state is a coexistence of ferromagnetic metal and antiferromagnetic charge-orbital ordered phases for LaBaMn$_2$O$_6$ and *A*-type antiferromagnetic metal for PrBaMn$_2$O$_6$ and NdBaMn$_2$O$_6$. These ground state behaviors are explained by the effect of Mn–O distance on the bandwidth and the layer structure with the RO–MnO$_2$–BaO–MnO$_2$ stacking along the *c*-axis.

1. Introduction

The discovery of novel structural and physical properties in the *A*-site ordered manganite RBaMn$_2$O$_6$ (R = Y and rare earth elements) has demanded new comprehension about perovskite manganese oxides.[1–8] The most significant structural feature of RBaMn$_2$O$_6$ is that the MnO$_2$ square sublattice is sandwiched by two types of rock-salt layers, RO and BaO, with much different sizes and consequently the MnO$_6$ octahedron itself is distorted, as schematically shown in Fig. 1. This means that the structural and physical properties of RBaMn$_2$O$_6$ can be no longer explained in terms of the basic structural distortion, the so-called tolerance factor f, as in the *A*-site disordered manganites $R_{0.5}A_{0.5}$MnO$_3$ (A = alkaline earth elements). Furthermore such a special deformation may give a new perturbation to the competition among charge, orbital, spin and lattice degrees of freedom. Previously we first reported the electronic phase diagram of RBaMn$_2$O$_6$ expressed as a function of the ratio of ionic radius of the *A*-site cations, r_{R3+}/r_{Ba2+} ($r_{Ba2+} = 1.61$ Å, $r_{R3+} \leq 1.36$ Å[9]).[3] Among possible combinations of R/Ba, the mismatch between RO and BaO is the smallest in La/Ba and the largest in Y/Ba. When R^{3+} is smaller than Sm^{3+}, the CE-type charge and orbital ordered (CO) state with a new stacking variation along the *c*-axis is stabilized at the relatively high temperatures (T_{CO}) far

above 300 K, which would be not only due to the absence of *A*-site randomness but also due to the tilt of MnO$_6$ octahedra as well as heavy distortions of MnO$_6$ octahedron.[2–5] Especially RBaMn$_2$O$_6$ (R = Tb, Dy, Ho and Y) shows the structural transition above T_{CO}, which is possibly accompanied by the d_{x2-y2} type orbital order.[2,3,5] On the other hand, RBaMn$_2$O$_6$ (R = La, Pr and Nd) with relatively larger R^{3+} has no octahedral tilt and shows a transition from a paramagnetic metal (PM) to a ferromagnetic metal (FM). Among perovskite manganese oxides studied so far, the structure without octahedral tilt is rare. As mentioned above, the MnO$_6$ octahedra have a noncentrosymmetric deformation. It is quite interesting how such deformation affect various interactions or competition among them. Since RBaMn$_2$O$_6$ (R = La, Pr and Nd) has a simple tetragonal structure with no tilt of MnO$_6$ octahedra, it is a good compound to study an effect of octahedral distortion on such competition. In this paper, we have refined the crystal structures and investigated the ground state properties of RBaMn$_2$O$_6$ (R = La, Pr and Nd). Neutron diffraction study together with magnetic susceptibility revealed interesting physical properties including electronic phase segregation.

2. Experimental Details

Powder samples of the *A*-site ordered RBaMn$_2$O$_6$ (R = La, Pr and Nd) were prepared by a solid-state reaction of La$_2$O$_3$, Pr$_6$O$_{11}$, Nd$_2$O$_3$, BaCO$_3$ and MnO$_2$ with 99.99% purities (Rare Metallic Inc.). Starting reagents were ground thoroughly, pressed into pellets and calcined in an Ar flow (6N) at 1573 K for 48 h. The use of Ar gas can avoid the formation of the *A*-site disorder. However, the obtained specimen contains a large amount of oxygen vacancy in the RO layer, providing RBaMn$_2$O$_{6-y}$ ($y \sim 1$). The metal ordering in the form of layers and the lack of oxygen in the RO layers are due to the general preference of the small R^{3+} ions to take eight-fold coordination. The second step is annealing the obtained specimen in flowing O$_2$ at 623 K for 48 h, which leads to the fully oxidation of the specimen, i.e., to RBaMn$_2$O$_6$.
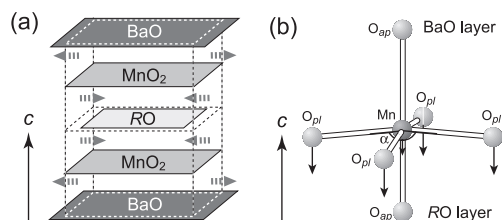
Fig. 1. (a) A schematic drawing of structural concept for the *A*-site ordered manganite RBaMn$_2$O$_6$. (b) An illustration of the distorted MnO$_6$ octahedron observed in RBaMn$_2$O$_6$.

*E-mail: t-nakaji@issp.u-tokyo.ac.jp

The X-ray powder diffraction experiments were performed using a MXP18 Mac Science diffractometer. The neutron powder diffraction experiments were conducted for $T = 20$–400 K using the Kinken powder diffractometer for high efficiency and high resolution measurements, HERMES, at Institute for Materials Research (IMR), Tohoku University, installed at the JRR-3M reactor in Japan Atomic Energy Research Institute (JAERI), Tokai, Japan. Neutrons with a wavelength of 1.8207 Å were obtained by the 331 reflection of the Ge monochromator. The $12'$-blank-sample-$18'$ collimation was employed. The magnetic properties were studied using a SQUID magnetometer in a temperature range $T = 2$–400 K. The magnetic ordered states at low temperatures were also studied by powder neutron diffraction.

3. Results

3.1 Crystal structures

The obtained products were checked to be single phase by X-ray diffraction. The order/disorder of R and Ba was carefully checked by the presence/absence of (0 0 1/2) reflection indexed in the primitive cell. Figure 2 shows the
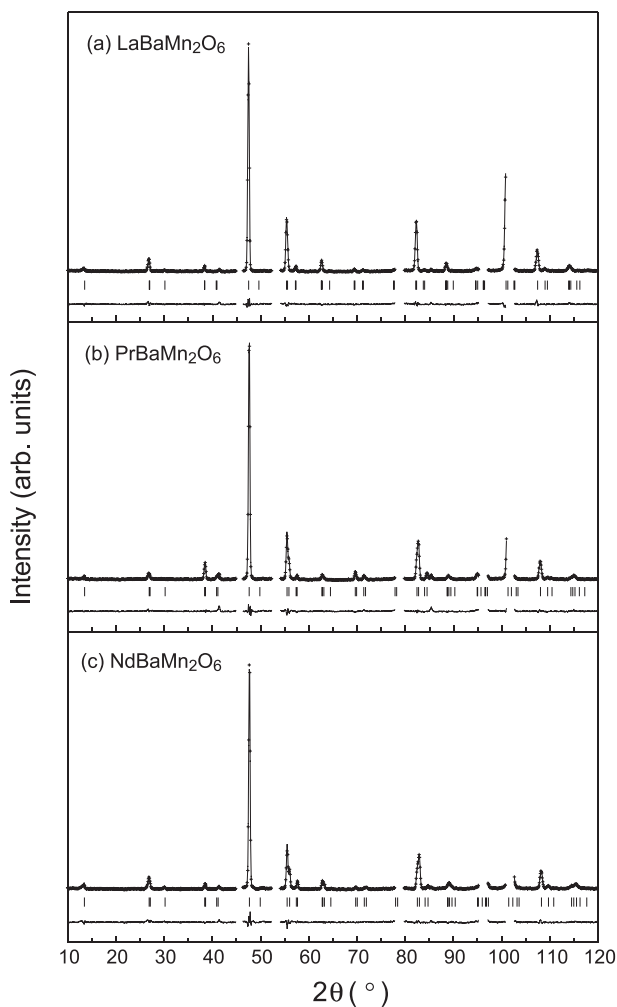
Fig. 2. Powder neutron diffraction profiles for (a) LaBaMn$_2$O$_6$, (b) PrBaMn$_2$O$_6$ and (c) NdBaMn$_2$O$_6$ at 400 K. The calculated and observed diffraction profiles are shown at the top with the solid line and the cross markers, respectively. The vertical marks in the middle show positions calculated for Bragg reflections. The lower trace is a plot of the difference between calculated and observed intensities.

Table I. Refined structural parameters for RBaMn$_2$O$_6$ (R = La, Pr and Nd) at 400 K.

	Atom	site	x	y	z	B_{iso} (Å^2)
LaBaMn$_2$O$_6$						
$a = 3.9178(1)$ Å	La	$1a$	0	0	0	0.6(1)
$c = 7.8070(5)$ Å	Ba	$1b$	0	0	$\frac{1}{2}$	0.8(2)
$V = 119.832(9)$ Å^3	Mn	$2h$	$\frac{1}{2}$	$\frac{1}{2}$	0.2451(13)	0.2(1)
$R_{\mathrm{wp}} = 10.87\%$	O(1)	$1c$	$\frac{1}{2}$	$\frac{1}{2}$	0	0.9(2)
$R_{\mathrm{e}} = 7.37\%$	O(2)	$4i$	$\frac{1}{2}$	0	0.2373(5)	1.0(1)
$R_{\mathrm{I}} = 9.79\%$	O(3)	$1d$	$\frac{1}{2}$	$\frac{1}{2}$	$\frac{1}{2}$	1.0(2)
$R_{\mathrm{F}} = 5.31\%$						
PrBaMn$_2$O$_6$						
$a = 3.9088(1)$ Å	Pr	$1a$	0	0	0	0.5(1)
$c = 7.7649(4)$ Å	Ba	$1b$	0	0	$\frac{1}{2}$	0.8(2)
$V = 118.639(9)$ Å^3	Mn	$2h$	$\frac{1}{2}$	$\frac{1}{2}$	0.2450(11)	0.2(1)
$R_{\mathrm{wp}} = 10.46\%$	O(1)	$1c$	$\frac{1}{2}$	$\frac{1}{2}$	0	0.9(2)
$R_{\mathrm{e}} = 6.83\%$	O(2)	$4i$	$\frac{1}{2}$	0	0.2333(5)	1.0(1)
$R_{\mathrm{I}} = 9.33\%$	O(3)	$1d$	$\frac{1}{2}$	$\frac{1}{2}$	$\frac{1}{2}$	1.0(2)
$R_{\mathrm{F}} = 8.56\%$						
NdBaMn$_2$O$_6$						
$a = 3.9043(1)$ Å	Nd	$1a$	0	0	0	0.6(1)
$c = 7.7448(3)$ Å	Ba	$1b$	0	0	$\frac{1}{2}$	0.6(2)
$V = 118.059(9)$ Å^3	Mn	$2h$	$\frac{1}{2}$	$\frac{1}{2}$	0.2445(12)	0.2(1)
$R_{\mathrm{wp}} = 9.67\%$	O(1)	$1c$	$\frac{1}{2}$	$\frac{1}{2}$	0	1.2(2)
$R_{\mathrm{e}} = 6.11\%$	O(2)	$4i$	$\frac{1}{2}$	0	0.2307(3)	1.1(1)
$R_{\mathrm{I}} = 9.92\%$	O(3)	$1d$	$\frac{1}{2}$	$\frac{1}{2}$	$\frac{1}{2}$	1.0(1)
$R_{\mathrm{F}} = 7.92\%$						

Note. All RBaMn$_2$O$_6$ (R = La, Pr and Nd) phases crystallize in space group $P4/mmm$ (No. 123).

neutron powder diffraction patterns of RBaMn$_2$O$_6$ (R = La, Pr and Nd) measured at 400 K. The crystal structures were refined by the Rietveld analysis of powder neutron diffraction using RIETAN 2000.[10] Independent refinement of the fractional occupancies of the Ba and R sites showed no antisite disorder to an experimental uncertainty of 3%. The refined unit cells parameters, positional coordinates, displacement parameters and refinement statistics are summarized in Table I. Table II demonstrates selected bond distances and angles.

The crystal structure at 400 K (PM state) has a tetragonal $a_{\mathrm{p}} \times a_{\mathrm{p}} \times 2c_{\mathrm{p}}$ cell with a space group of $P4/mmm$, where a_{p} and c_{p} denote the primitive cell for the simple cubic perovskite, and has no tilt of MnO$_6$ octahedra which is rare in manganese perovskites. On the other hand, the MnO$_6$ octahedron itself is distorted in a way as illustrated in Fig. 1(b): Both Mn and oxygen atoms (O$_{\mathrm{pl}}$) in the MnO$_2$ plane are displaced toward the RO layer to a larger extent for O$_{\mathrm{pl}}$. As a result, the angle of $\angle$O$_{\mathrm{pl}}$–Mn–O$_{\mathrm{pl}}$ [$=\angle\alpha$, see Fig. 1(b)] deviates from $180°$ to $176.4°$ (La), $174.7°$ (Pr) and $173.7°$ (Nd), while that of $\angle$O$_{\mathrm{ap}}$–Mn–O$_{\mathrm{ap}}$ (O$_{\mathrm{ap}}$: apical oxygen atom) is $180°$ in all compounds. The distance of Mn–O$_{\mathrm{ap}}$ is shortened (1.913 Å for La, 1.902 Å for Pr and 1.894 Å for Nd) in the RO side, while that is elongated (1.989 Å for La, 1.979 Å for Pr and 1.978 Å for Nd) in the BaO side. Intermediate values are obtained for the distance of Mn–O$_{\mathrm{pl}}$ (1.960 Å for La, 1.956 Å for Pr and 1.955 Å for Nd).

3.2 Magnetic properties

The magnetic susceptibilities (M/H) of RBaMn$_2$O$_6$ (R =

Table II. Selected interatomic distances and angles of RBaMn$_2$O$_6$ (R = La, Pr and Nd) at 400 K.

LaBaMn$_2$O$_6$ distances (Å)		PrBaMn$_2$O$_6$ distances (Å)		NdBaMn$_2$O$_6$ distances (Å)	
Mn–O(1)	1.913(10) × 1	Mn–O(1)	1.902(7) × 1	Mn–O(1)	1.894(6) × 1
Mn–O(2)	1.960(1) × 4	Mn–O(2)	1.956(1) × 4	Mn–O(2)	1.955(1) × 4
Mn–O(3)	1.989(10) × 1	Mn–O(3)	1.979(7) × 1	Mn–O(3)	1.978(7) × 1
Mn–O (average)	1.957	Mn–O (average)	1.952	Mn–O (average)	1.947
angles (°)		angles (°)		angles (°)	
Mn–O(1)–Mn	180	Mn–O(1)–Mn	180	Mn–O(1)–Mn	180
Mn–O(2)–Mn	176.4(7)	Mn–O(2)–Mn	174.7(6)	Mn–O(2)–Mn	173.7(6)
Mn–O(3)–Mn	180	Mn–O(3)–Mn	180	Mn–O(3)–Mn	180
O(1)–Mn–O(3)	180	O(1)–Mn–O(3)	180	O(1)–Mn–O(3)	180
O(2)–Mn–O(2)	176.4(7)	O(2)–Mn–O(2)	174.7(6)	O(2)–Mn–O(2)	173.7(6)
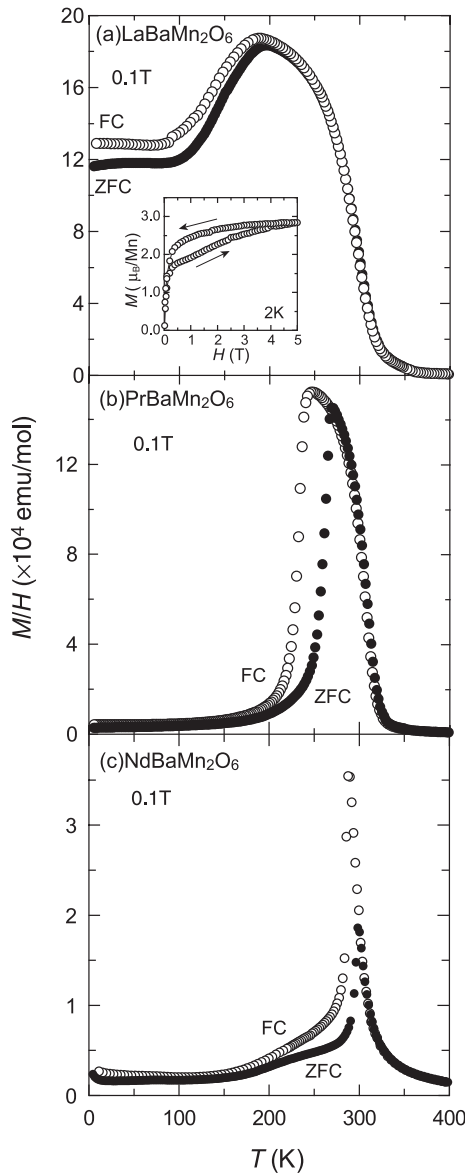
Fig. 3. Temperature dependence of magnetic susceptibilities for RBaMn$_2$O$_6$ with R = La (a), Pr (b) and Nd (c). The magnetization was measured under 0.1 T on zero-field cooled (ZFC) and field cooled (FC) processes. The inset in Fig. 3(a) shows the magnetization curves of LaBaMn$_2$O$_6$ at 2 K.
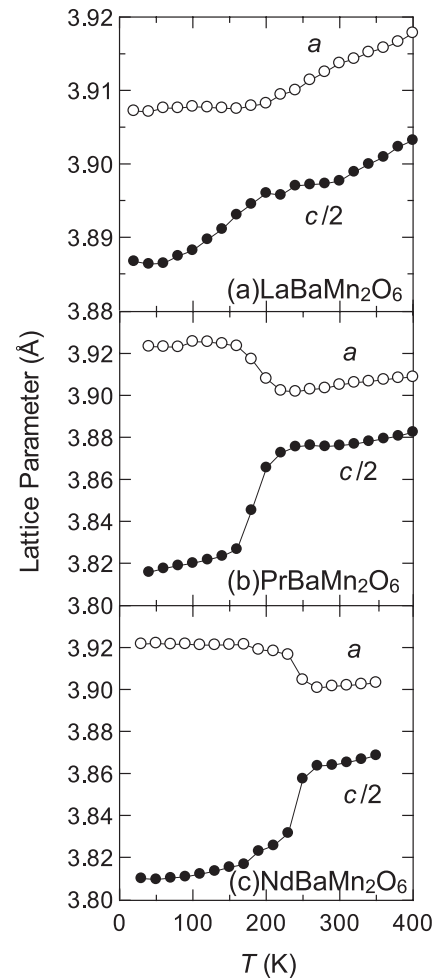
Fig. 4. Temperature dependence of lattice parameters for (a) LaBaMn$_2$O$_6$, (b) PrBaMn$_2$O$_6$ and (c) NdBaMn$_2$O$_6$.

La, Pr and Nd) are shown in Fig. 3. As can be seen in Fig. 3(a), LaBaMn$_2$O$_6$ transforms to ferromagnetic metal (F) at T_C = 330 K,[1] accompanying with a sharp increase of M/H but without any structural change. The M/H then starts to decrease at 200 K, where only slight change of lattice parameters is observed [Fig. 4(a)], and becomes constant below 100 K, agreeing with the previous report.[1] However, the neutron diffraction study reveals an unexpected phenomenon that the CE-type antiferromagnetic CO phase [AFI(CE)] coexists with the FM phase as the ground state of LaBaMn$_2$O$_6$, as shown in Fig. 5(a). Figure 6 shows the
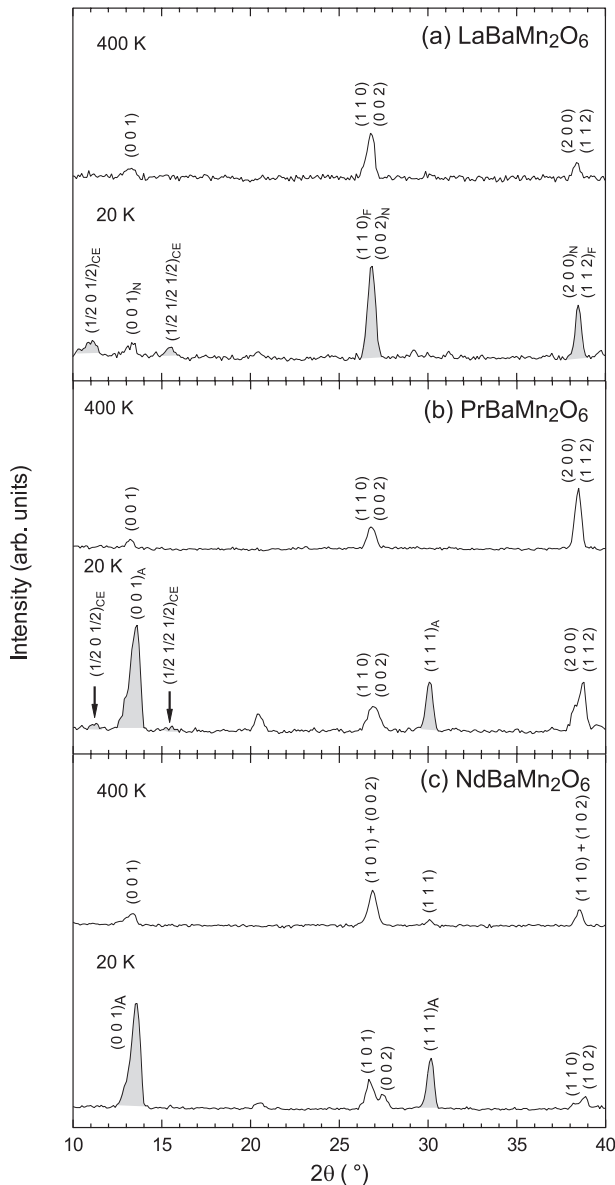
Fig. 5. (a) Neutron diffraction patterns of powdered (a) LaBaMn$_2$O$_6$, (b) PrBaMn$_2$O$_6$ and (c) NdBaMn$_2$O$_6$ at 400 K and 20 K. The indexes (hkl)$_F$, (hkl)$_A$ and (hkl)$_{CE}$ represent the peaks characteristic of ferromagnetic metal, A-type antiferromagnetic metal and CE-type charge/orbital ordered antiferromagnetic states, respectively.

Fig. 6. Temperature dependence of the intensity of peaks, (110)$_F$, (001)$_A$ and (1/2 1/2 1/2)$_{CE}$ for (a) LaBaMn$_2$O$_6$, (b) PrBaMn$_2$O$_6$ and (c) NdBaMn$_2$O$_6$.

intensity of neutron diffraction peaks for RBaMn$_2$O$_6$ (R = La, Pr and Nd) as a function of temperature. The AFI(CE) phase appears below $T_t = 200$ K [Fig. 6(a)], in accordance with the reduction of M/H. A similar coexistence has been observed in $R_{1-x}A_x$MnO$_3$ so far and attributed to the A-site randomness or fluctuation of composition.[11] Since the present system does not have such randomness, the observed electronic phase segregation is an essential behavior caused by the interplay among spin, charge, orbital and lattice degrees of freedom and might be explained by the effect of Mn–O distance on the bandwidth, as discussed in the next section. Interestingly this AFI(CE) phase is converted to the FM phase under external magnetic field, as shown in the inset of Fig. 3(a). The volume fraction of the AFI(CE) phase is estimated to be about 30% from the difference of magnetization between 0.3 T and 5 T at 2 K. A similar behavior has been observed in $R_{1-x}A_x$MnO$_3$.[11] On the other

hand, PrBaMn$_2$O$_6$ and NdBaMn$_2$O$_6$ show the PM-to-FM transition at $T_C = 310$ K (Pr) and 300 K (Nd), followed by the magnetic transition at 270 K (Pr) and 290 K (Nd) accompanied by the large reduction of M/H [Fig. 3(b) and 3(c)]. The neutron diffraction study reveals the transition from FM to A-type antiferromagnetic metal [AFM(A)] at $T_N = 270$ K (Pr) and 290 K (Nd) (Figs. 5 and 6). This transition associated with d_{x2-y2} orbital order is consistent with the change of lattice parameters observed, namely the elongation of the a-axis and the contraction of the c-axis at T_N, as shown in Fig. 4(b) and 4(c). The neutron diffraction pattern for PrBaMn$_2$O$_6$ below $T_t = 150$ K shows the coexistence of a slight amount of AFI(CE), while no trace of AFI(CE) phase is seen in NdBaMn$_2$O$_6$.

4. Discussion

Figure 7 shows the electronic phase diagram of
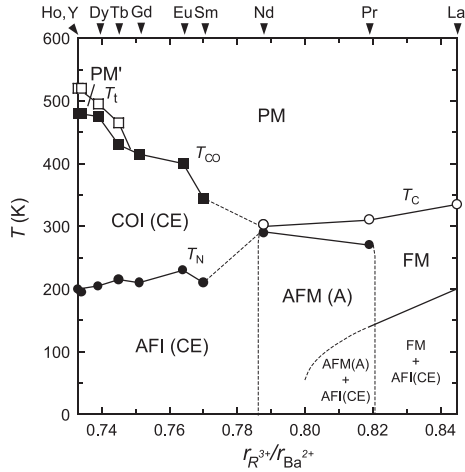
Fig. 7. Electronic phase diagram for $R\text{BaMn}_2\text{O}_6$. FM: ferromagnetic metal phase, AFM(A): A-type antiferromagnetic metal phase, AFI(CE): antiferromagnetic CE-type charger/orbital ordered insulator phase, COI(CE): CE-type charger/orbital ordered insulator phase, PM: paramagnetic metal phase.

$R\text{BaMn}_2\text{O}_6$ ($R = $ Y and rare earth elements) renewed by adding the present results to the previous one. In spite of apparent similarity to the phase diagram of $R_{0.5}A_{0.5}\text{MnO}_3$,[12] there are several significant differences. In the phase diagram of $R_{0.5}A_{0.5}\text{MnO}_3$, there exists a critical region where the FM and CO interactions compete with each other and therefore the transition from FM to AFI(CE) as a function of temperature, which is responsible for colossal magnetoresistance, is observable. If the ratio r_{R3+}/r_{Ba2+} were an appropriate measure of the bandwidth as is the case of f for $R_{0.5}A_{0.5}\text{MnO}_3$, such a critical region would be located between $\text{SmBaMn}_2\text{O}_6$ and $\text{NdBaMn}_2\text{O}_6$, and a FM-to-AFI(CE) transition would be expected in $\text{NdBaMn}_2\text{O}_6$ adjacent to $\text{SmBaMn}_2\text{O}_6$. In reality, however, the ground state of $\text{NdBaMn}_2\text{O}_6$ is the AFM(A) phase and a fractional transition from FM to AFI(CE) is observed in $\text{LaBaMn}_2\text{O}_6$ far from $\text{SmBaMn}_2\text{O}_6$. This implies that $\text{LaBaMn}_2\text{O}_6$ might be located closer to the CO state and the bandwidth would become larger as $\text{LaBaMn}_2\text{O}_6 < \text{PrBaMn}_2\text{O}_6 < \text{NdBaMn}_2\text{O}_6$.

Here it should be noticed again that $R\text{BaMn}_2\text{O}_6$ ($R = $ La, Pr and Nd) has no tilt of MnO_6 octahedra. It is known that the tilt of MnO_6 octahedra in ordinary manganese perovskites occurs in order to fit the larger MnO_2 sublattice to the smaller $A\text{O}$ sublattice ($f < 1$). No tilt of MnO_6 octahedra is expected to occur either when the MnO_2 lattice has the almost same size as the $A\text{O}$ lattice ($f \approx 1$) or when the MnO_2 lattice is expanded by the $A\text{O}$ lattice ($f > 1$). In $R\text{BaMn}_2\text{O}_6$ ($R = $ La, Pr, Nd) with relatively larger R^{3+}, the expansion of the MnO_2 lattice by the much larger BaO lattice ($f = 1.071$) should overwhelm the contraction by the smaller $R\text{O}$ lattice ($f = 0.982$ for LaO, $f = 0.964$ for PrO and $f = 0.950$ for NdO), in contrast to the case of $R\text{BaMn}_2\text{O}_6$ with $R = $ Sm and later rare earth elements. Actually, the Mn–O_{pl} distance ($\sim 1.96\,\text{Å}$) is elongated compared with that (1.91–$1.94\,\text{Å}$) for the regular $\text{Mn}^{3.5+}\text{O}_6$. The increase of Mn–$\text{O}_{\text{pl}}$ distance and the deviation of the angles $\angle\text{Mn–O}_{\text{pl}}\text{–Mn}$ and $\angle\text{O}_{\text{pl}}\text{–Mn–O}_{\text{pl}}$ from $180°$ would result in the decrease of bandwidth.

In addition, the alternate stacking of $R\text{O}$ and BaO layers

would provide another important feature, that is a two-dimensional character in the structure, which would be preferable for the d_{x2-y2} type orbital order [AFM(A)]. These structural characteristics explain well the present results; No tilt structure stabilizes FM but the two-dimensional character in the structure leads to AFM(A) associated with d_{x2-y2} type orbital order as the ground states of $\text{NdBaMn}_2\text{O}_6$ and $\text{PrBaMn}_2\text{O}_6$. The larger elongation of Mn–O_{pl} distance in $\text{LaBaMn}_2\text{O}_6$ destabilizes FM to some extent as a result of the decrease of bandwidth and results in the fractional transition from FM to AFI(CE) [coexistence of FM and AFI(CE) phases as the ground state]. The effect of Mn–O_{pl} distance on the bandwidth has never been seen nor discussed in the ordinal perovskite manganese oxides, because they have finite tilt of MnO_6 octahedra, by which the bandwidth is dominantly controlled.

Lowering of both T_{C} and T_{CO} in the critical region as observed $R_{0.5}A_{0.5}\text{MnO}_3$ is not recognized in the phase diagram of $R\text{BaMn}_2\text{O}_6$. The absence of such behavior in $R\text{BaMn}_2\text{O}_6$ is partly due to the absence of the A-site randomness. In the critical region, the FM [AFM(A)] and CO interactions compete with each other and are significantly affected by composition, coherent size of crystal, external field *etc.* The FM [AFM(A)] and CO interactions are distributed in $R_{0.5}A_{0.5}\text{MnO}_3$ with the A-site randomness. Such fluctuation of interactions enhances the criticality. On the other hand, it could be more definite which interaction becomes dominant in $R\text{BaMn}_2\text{O}_6$ without the A-site randomness.

5. Summary

To summarize, we have investigated the structures and electromagnetic properties of the A-site ordered manganite $R\text{BaMn}_2\text{O}_6$ ($R = $ La, Pr and Nd). The most significant structural feature of the A-site ordered manganese perovskites, $R\text{BaMn}_2\text{O}_6$ ($R = $ Y and rare earth elements), is that the MnO_2 square sublattice is sandwiched by two types of rock-salt layers, $R\text{O}$ and BaO, with much different sizes and consequently the MnO_6 octahedron itself is distorted in a noncetrosymmetric manner. The crystal structure of the $R\text{BaMn}_2\text{O}_6$ ($R = $ La, Pr and Nd) has a tetragonal $a_{\text{p}} \times a_{\text{p}} \times 2c_{\text{p}}$ cell with a space group of $P4/mmm$, where a_{p} and c_{p} denote the primitive cell for the simple cubic perovskite, and has no tilt of MnO_6 octahedra which is rare in manganese perovskites. Reflecting the crystal structures, the ferromagnetic double exchange interaction is dominant in $R\text{BaMn}_2\text{O}_6$ ($R = $ La, Pr and Nd), but the ground state is a mixture of FM and AFI(CO) for $\text{LaBaMn}_2\text{O}_6$ and A-type AFM for $\text{PrBaMn}_2\text{O}_6$ and $\text{NdBaMn}_2\text{O}_6$. These ground state behaviors are explained by the effect of Mn–O distance on the bandwidth and the two-dimensional character in the structure.

1) F. Millange, V. Caignaert, B. Domengés, B. Raveau and E. Suard: Chem. Mater. **10** (1998) 1974.
2) T. Nakajima, H. Kageyama and Y. Ueda: J. Phys. Chem. Solids **63** (2002) 913.
3) T. Nakajima, H. Kageyama, H. Yoshizawa and Y. Ueda: J. Phys. Soc. Jpn. **71** (2002) 2843.
4) H. Kageyama, T. Nakajima, M. Ichihara, Y. Ueda, H. Yoshizawa and K. Ohoyama: J. Phys. Soc. Jpn. **72** (2003) 241.
5) T. Nakajima, H. Kageyama, K. Ohoyama, H. Yoshizawa and Y. Ueda: to be published in J. Solid State Chem.
6) S. V. Trukhanov, I. O. Troyanchuk, M. Hervieu, H. Szymczak and K. Barner: Phys. Rev. B **66** (2002) 184424.
7) M. Uchida, D. Akahoshi, R. Kumai, Y. Tomioka, T. Arima, Y. Tokura and Y. Matsui: J. Phys. Soc. Jpn. **71** (2002) 2605.
8) T. Arima, D. Akahoshi, K. Oikawa, T. Kamiyama, M. Uchida, Y. Matsui and Y. Tokura: Phys. Rev. B **66** (2002) 140408.
9) R. D. Shannon and C. T. Prewitt: Acta Crystallogr. B **25** (1969) 925.
10) F. Izumi and T. Ikeda: Mater. Sci. Forum **321–324** (2000) 198.
11) H. Kawano, R. Kajimoto, H. Yoshizawa, Y. Tomioka, H. Kuwahara and Y. Tokura: cond-mat/9808286.
12) See for reviews, C. N. R. Rao and B. Raveau: *Colossal Magneto-resistance, Charge Ordering and Related Properties of Manganese Oxides* (World Scientific, Singapore, 1998).